



Expression, purification, characterization and in silico analysis of newly isolated hydrocarbon degrading bleomycin resistance dioxygenase

Vinay Sharma¹ · Rajender Kumar² · Vishal Kumar Sharma³ · Ashok kumar Yadav³ · Marja Tiirola⁴ · Pushpender Kumar Sharma¹

Received: 9 July 2019 / Accepted: 23 October 2019
© Springer Nature B.V. 2019

Abstract

In the present investigation, we report cloning, expression, purification and characterization of a novel Bleomycin Resistance Dioxygenase (BRPD). His-tagged fusion protein was purified to homogeneity using Ni-NTA affinity chromatography, yielding 1.2 mg of BRPD with specific activity of 6.25 U mg⁻¹ from 600 ml of *E. coli* culture. Purified enzyme was a dimer with molecular weight ~ 26 kDa in SDS-PAGE and ~ 73 kDa in native PAGE analysis. The protein catalyzed breakdown of hydrocarbon substrates, including catechol and hydroquinone, in the presence of metal ions, as characterized via spectrophotometric analysis of the enzymatic reactions. Bleomycin binding was proven using the EMSA gel retardation assay, and the putative bleomycin binding site was further determined by in silico analysis. Molecular dynamic simulations revealed that BRPD attains octahedral configuration in the presence of Fe²⁺ ion, forming six co-ordinate complexes to degrade hydroquinone-like molecules. In contrary, in the presence of Zn²⁺ ion BRPD adopts tetrahedral configuration, which enables degradation of catechol-like molecules.

Keywords Metagenomics · Dioxygenase · Aromatic hydrocarbons · Pesticides · Pollutant · Molecular modelling

Introduction

Aromatic hydrocarbons (AHs) including pesticides are highly toxic compounds and are major chemical hazards discharged into surroundings from different sources, including agricultural and industrial wastes [1–3]. These pollutants are very stable within the surroundings, and the existing

physico-chemical techniques are often inefficient in removing them. Bioremediation, a cost-effective technique that involve microbes can remove these persistent environmental pollutants via enzymatic catabolism [4]. Soil bacteria especially uncultured subset are potential catalytic sources for biodegradation of aromatic hydrocarbons [5]. Ring-cleaving dioxygenases play an important role in aromatic metabolism, both in eukaryotes and prokaryotes. These dioxygenases are classified as intradiol dioxygenases which catalyzes ortho cleavage and extradiol dioxygenases which catalyze meta cleavage. Both classes of enzymes have distinct features and specificities [4]. The extradiol dioxygenases are generally more versatile, cleaves broader number of substrates including antibiotics [3, 5]. In this category, hydroquinone dioxygenases (HQDO) are key enzymes as they act on hydroquinone (HQ), a key intermediate of several aromatic hydrocarbons such as 4-nitrophenol [6, 7], γ -hexachlorocyclohexane [8], 4-hydroxyacetophenone [9] and 4-aminophenol [10]. Hydroquinone dioxygenases (HQDOs) are divided into 2 subtypes sharing few similarities [11]. Members of type I dioxygenases are phylogenetically correlated with the well-described extradiol catechol

Electronic supplementary material The online version of this article (<https://doi.org/10.1007/s11033-019-05159-x>) contains supplementary material, which is available to authorized users.

✉ Pushpender Kumar Sharma
pushp_78@rdiffmail.com

¹ Department of Biotechnology, Sri Guru Granth Sahib World University, Fatehgarh Sahib, Pb, India

² Department of Clinical Microbiology, Umeå University, 90185 Umeå, Sweden

³ PGI, Chandigarh, India

⁴ Department of Biological and Environmental Science, Nanoscience Center, University of Jyväskylä, 40014 Jyväskylä, Finland

dioxygenases [12] and share similarity with VOC (vicinal oxygen chelate) superfamily [13] that harbour highly conserved structural motif ($\beta\alpha\beta\beta$) [14]. Some of the extradiol dioxygenases like 2,3-dihydroxybiphenyl 1,2-dioxygenase and catechol 2,3-dioxygenase are part of the same superfamily [5, 15]. All these proteins belong to VOC superfamily and contain a 2-His-1-carboxylate metal binding motif. These proteins use variety of mechanisms to hamper the effects of antibiotics including bleomycin [16]. Bleomycin resistance protein (BRP) share homology with this superfamily and confer bleomycin activity [17]. Type II hydroquinone dioxygenases accommodate two different subunits of $\alpha_2\beta_2$, forming a hetero-tetramer. These enzymes cleave HQs formed during degradation pathway of hydroxyacetophenone [9] and p-nitrophenol [18, 19]. Type II hydroquinone dioxygenase from *Pseudomonas fluorescens* ACB, *Pseudomonas* sp. WBC3 (PnpCD) *Sphingomonas* sp. TTNP3, *Burkholderia* sp. SJ98, *Pseudomonas* sp. 1–7, have been purified and partially characterized so far [9, 11, 19, 20]. Members of this family are structurally well characterized, and are known to be part of the cupin superfamily, one of the most functionally diverse protein classes [21]. However, both the cupin β -barrel fold and the paired $\beta\alpha\beta\beta$ modules of the VOC superfamily proteins forms a scaffold for a metal coordination environment [21, 22].

Herein, we report expression, purification and characterization of a novel type I hydroquinone dioxygenase which showed >95% similarity with bleomycin (antimitotic-antibiotic) resistance proteins, the gene was cloned from metagenomic DNA extracted from contaminated agricultural soil.

Materials and methods

Expression and purification of BRPD

BRPD full length gene sequence was amplified using specific primers containing Bam HI (F-5'-CGGGATCCAACCAATTAAGG-3' and XhoI site R-5'-GTACTCGAGCTCTTTAATAAATT). These primers were designed based on the sequence information of a partial fragment (Accession no. MH643810) amplified previously in our lab from metagenomic DNA using degenerate set of primers. Sequencing and bioinformatic analysis of the partial DNA fragment revealed that it had shared more than 95% sequence similarity with uncharacterized bleomycin resistant dioxygenase of *B. Cereus*. Double digested full-length gene was ligated in frame with the BamHI and XhoI digested pET23a containing C-terminal six-His-tag. The recombinant plasmid transformed in *E. coli* BL21 (DE3) carrying BRPD was grown in Luria Broth (LB) at 37 °C till OD_{600} reaches 0.6. After that, the plasmid DNA was extracted from B121(DE3) manually and sequenced. Full

length gene sequence was provided a gene accession number MK766458.1 for nucleotide sequence of BRPD while QED41507 for full length protein sequence. Further, the culture was induced for 4 h by addition of 1 mM isopropyl- β -D-thiogalactopyranoside (IPTG) at 37 °C. Cells were harvested by centrifugation, lysed and suspended in the binding buffer. The soluble fraction was then used for purification of recombinant protein using nickel-nitrilotriacetic acid (Ni^{2+} -NTA) agarose (Merck Biosciences). Binding buffer consists of 500 mM NaCl, 10 mM imidazole, and sodium phosphate buffer (250 mM, pH 8.0). The elution buffer contained all above buffer components except that the final concentration of imidazole was 50 mM, 100 mM and 150 mM. Protein concentration was determined according to the Lowry method with bovine serum albumin as the standard. The eluted fractions were aliquot and stored in 50% glycerol at -70 °C. All purification steps were performed at 4 °C unless and otherwise stated.

Enzyme activity assay

Enzyme activity was routinely measured at 25 °C in the UV-VIS spectrophotometer (Perkin Elmer, Hitachi) by monitoring the formation of 4-hydroxymuconic semialdehyde at 320 nm ($\epsilon_{320} = 11.0 \text{ mM}^{-1} \text{ cm}^{-1}$) [6, 23]. One unit of enzyme activity was defined as the production of 1 μmol 4-hydroxymuconic semialdehyde per minute. The assay mixture (1.0 ml) typically contained 10 mM hydroquinone, 1 mM $ZnSO_4$, 1 mM $FeSO_4$ 0.8–10 μg of protein and 50 mM phosphate buffer (pH 7.4). The reference cuvette contained all of these compounds except the substrate, and as the enzyme was subject to suicide deactivation upon incubation with HQ, only initial rates were recorded within 20 s. Enzyme activity for other aromatic substrate like catechol was also measured within 1 h incubation at 30 °C in the presence of Zn^{2+} (1 mM), phosphate buffer (50 mM, pH 7.4) at different concentrations of 10 mM and 50 mM by monitoring the formation of 2-hydroxymuconic semi-aldehyde at 375 nm ($\epsilon = 33.400 \text{ mM}^{-1} \text{ cm}^{-1}$).

Enzyme inhibition assay

Time-dependent inhibition of BRPD was determined by incubating purified enzyme at 25 °C in the presence of 20 mM 4-hydroxy benzoate (4-HBA), *para*-nitrophenol (PNP) and phenol for 1 h followed by addition of hydroquinone (10 mM) to measure its degradation within 20 s.

BRPD-bleomycin molecule binding assay

The binding affinity of BRPD to bleomycin (Sigma-Aldrich) was confirmed by electrophoretic mobility shift assay (EMSA) where purified BRPD (10 μg) was incubated with

increased concentrations of bleomycin (10, 20, 30 μg) in 30 μl of Tris–HCl (10 mM, pH 7.5) at 16 $^{\circ}\text{C}$. After 3 h incubation, 30 μl of reaction mixture was loaded onto a 12% non-denaturing polyacrylamide gel, as described previously [17, 24].

Molecular diversity analysis

Nearly 1000 sequences were retrieved from Uniprot database after performing Basic Local Alignment Search Tool (BLAST) of queried sequence (BRPD). Sequence redundancy was removed at 75% sequence identity for set of representative sequences, these sequences also includes protein sequences for which crystal structure is available. Multiple sequence alignment (MSA) was performed using the MUSCLE program. The molecular evolutionary history was inferred using Neighbor-Joining method [25]. The evolutionary distances were computed using the Poisson correction method [26] and included units of the number of amino acid substitutions per site, analysis involved 25 amino acid sequences. All ambiguous positions were removed from the comparison. There was a total of 350 positions in the final dataset. Evolutionary analysis was performed using MEGA 7 [27], and the secondary structure prediction was done using I-TEASSER [28].

Analysis of evolutionary conserve sequences

For comprehensive analysis of evolutionary conserve sequences, ConSurf Program [29, 30] was used. The primary protein sequence of BRPD was queried to search homologues sequences in protein database UNIREF-90 (<http://www.uniprot.org/help/uniref>) using HMMER (hidden Markov models) homolog search algorithm with E-value cutoff 0.0001. Best top 500 hits were used for Multiple Sequence Alignment (MSA). The MSA was performed using the MAFFT program. All other parameters were kept at default values for calculation of conservation scores.

Structural modelling and molecular dynamics simulation studies

Since the target protein structure was not reported in the PDB database, therefore comparative protein modelling was performed using highly identical template structures (PDB ID: 1ZSW) via SWISS-MODEL server (<https://swissmodel.expasy.org>) including metal ion coordinates. Modelled protein structure was energy minimized by 100 steps steepest descent method following 50 steps of conjugate gradient method in minimize structure module of USCF Chimera software [31]. The minimized modelled structures as well as the close structural homolog's protein structure were simulated incusing different metal ions (Zn^{2+} , Fe^{2+}) by

performing MD simulation in AMBER 16.0 software package using ff14SB force fields [32]. Using the t leap module, all required parameters were applied, considering ionisable residues set at their default protonation states at pH 7 value. Each system was neutralized by adding $\text{Na}^{+}/\text{Cl}^{-}$ ions and solvated in a truncated octahedron box of TIP3P [33] water model with a margin distance of 10 \AA . For long-range Coulombic interactions calculation, the particle mesh Ewald method was used [34]. The SHAKE algorithm [35] was employed to restrain all atoms covalently bonded to hydrogen atoms. The protocol was adopted that previous describe by author [36] for system minimization, equilibrium, etc. Finally, a MD simulation production was run for 100 ns using NPT ensemble at room temperature with 1.0 atm pressure. Coordinate trajectories were saved every 20 ps and further analyzed using VMD programs.

Molecular docking studies

Molecular docking studies of experimental tested substrates were performed using the AUTODOCK 4.2 program. The substrates and refined modelled protein molecule were analyzed using standard docking ligand and protein files preparation protocols. The docking protocol was set as per previous reported studies [37]. The grid size was set as follows, it includes the metal ion and complete active site. The docking conformations were set to 30 and all other docking parameters were set to default values. All 30 docked conformations were analyzed.

Results

Expression and purification of BRPD

Recombinant BRPD was over expressed in *E. coli* BL21 (DE3) as C-terminal His-tagged fusion protein. The expressed and purified protein as analyzed in 12% SDS-PAGE showed induction of distinct protein band with an apparent molecular mass of ~ 26 kDa as detected on SDS-PAGE (Fig. 1a). The purified protein band as depicted in Fig. 1b do not fit to molecular mass of BRPD as deduced from its amino acid sequence (36.8 kDa). Interestingly, native PAGE revealed size ~ 73 kDa protein band indicating dimeric nature of protein (Fig. 1c). Furthermore, we embarked upon investigating the electrophoretic mobility shift assay (EMSA) using purified BRPD which showed that the BRPD protein migration was delayed in the presence of bleomycin-like molecules in concentration dependent manner (Fig. 1d). Altogether, Ni–NTA based purification of recombinant protein resulted in large quantities of soluble and active BRPD from a 600 ml culture having specific activity of 6.25 U mg^{-1} as depicted in Table 1.

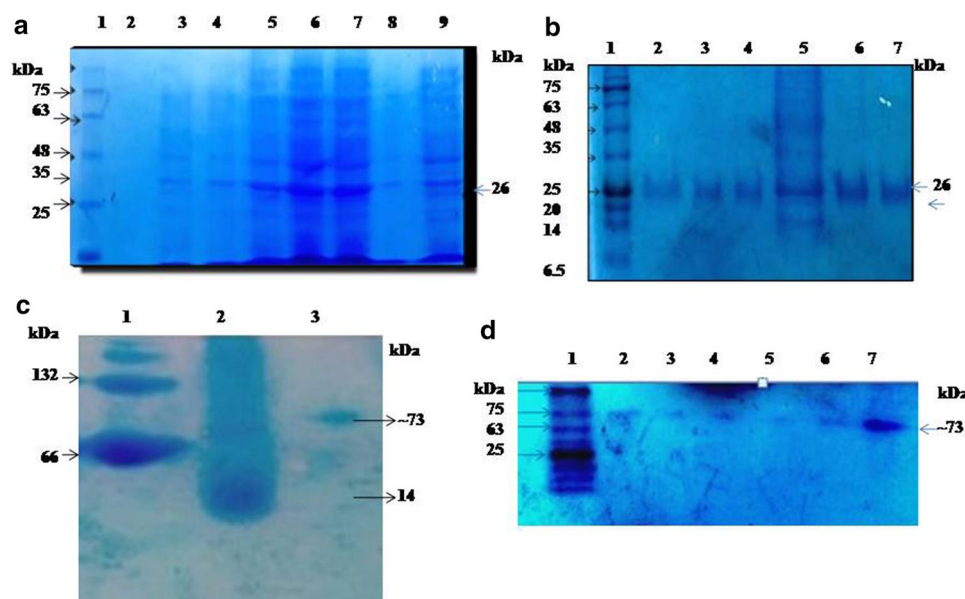


Fig. 1 SDS-PAGE of BRPD. **a** Lane 1: Molecular mass standards (molecular masses in kDa) are indicated on the left; lane 2 and 8: Empty well, lane 3–4 cell extracts of uninduced *E. coli* BL21 containing pET23a; lane 5,6,7, and 9: Cell extracts of induced *E. coli* BL21 containing pET23a with BRPD at different time interval (30 min 1 h, 2 h, 3 h, 4 h). **b** lane1: Molecular weight marker, lane 2,3 and 4 puri-

fied protein sample lane 5 induced protein sample lane 6–7 purified protein sample **c** Native page of BRPD; lane1,BSA; lane 2 Lysozyme; lane 3 purified BRPD bands. **d** EMSA of purified BRPD and with varying concentration of bleomycin (lane1-Protein molecular weight marker, lane 2–5: 10, 20, 30 and 40 μg bleomycin + 10 μg BRPD respectively, lane 6: 10 μg BRPD alone)

Table 1 Purification profile of BRPD

Purification step	Activity U/ml	Protein (mg)	Specific act. (U mg^{-1})	Purification fold	Yield
Cell Lysate	30.5	16.2	1.88	1	100
Ni-NTA	14.8	3.3	4.48	2.38	48.52
Dialysis	7.5	1.2	6.25	3.32	24.6

Catalytic activity

BRPD catalyzes ring cleavage of hydroquinone to 4-hydroxymuconic semi aldehyde and exhibited very narrow optimal pH values ranging from 7.4 to 8.0 in phosphate buffer, no activity was observed in the Tris buffer. More interestingly, we observed low activity of BRPD towards hydroquinone in the absence of metal ions. Figure 2a shows absorption spectrum of Hydroquinone, showing a prominent peak at 289 nm, however, on incubation with Zn^{2+} (1 mM) and Fe^{2+} (1 mM), there is emergence of peak at 320 nm which indicates conversion of Hydroquinone to 4-hydroxymuconic semi aldehyde, the enzyme shows activity in presence of Zn^{2+} (1 mM) and Fe^{2+} (1 mM) indicating its metal dependent nature as shown in Fig. 2b, interestingly Zn^{2+} ion alone was also found to be equally active as depicted in Fig. 2c and ~ fourfold increased activity was observed in the presence of Zn^{2+} alone. This may indicate tight dependency of the BRPD

towards zinc than iron, which may be attributed to oxidation of ferrous iron to ferric iron, which could be or not be restored by adding Fe(II) ions, as reported previously [11, 13]. BRPD also catalyzes conversion of catechol to 2-hydroxymuconic semi aldehyde evidenced from emergence of peak at 375 nm, in presence of Zinc, these results indicates its substrate versatility as well as more specificity towards zinc ion (Fig. 2D). Further, BRPD also showed hydroquinone degradation in presence of other divalent metals ions that includes Hg^{2+} , Mg^{2+} , Cu^{2+} with activity (%) (i.e., relative absorbance increases and decrease at 320 nm as compared to Zn^{2+} absorbance) of 96.5, 70.17 and 35.08 respectively (Table 2). Furthermore, activity of BRPD was strongly inhibited (> 80% inhibition) in presence of substrate analogue like *para* nitro phenol but not by 4-HBA (< 2% inhibition) indicating the role of electron withdrawing (OH functional group) and electron donating substituent's (-Nitro functional group) in *para* to the hydroxyl group located adjacently to the cleaving site as it

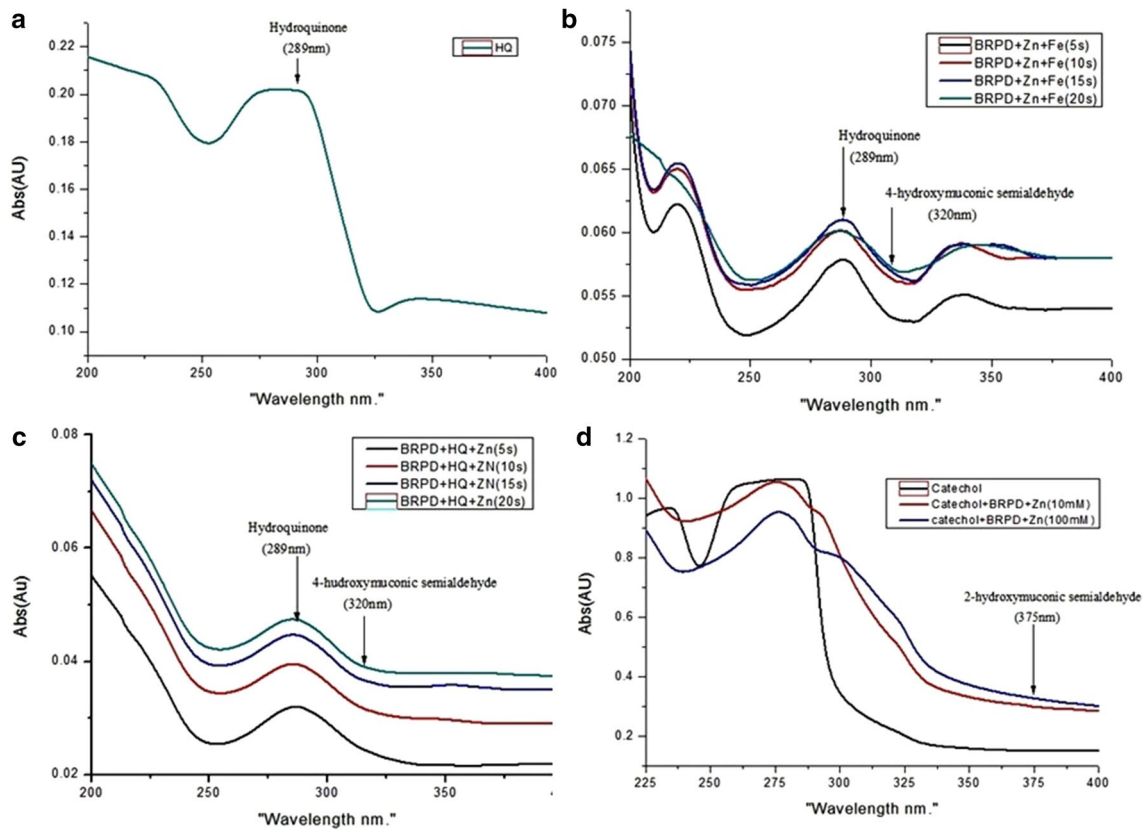


Fig. 2 Spectrophotometric measurement of hydroquinone and catechol degradation by BRPD **a** Standard hydroquinone absorbance spectra **b** Spectra recorded during catalytic conversion of hydroquinone using BRPD in presence of Zn^{2+} ions and Fe^{2+} ions **c** Spectra

recorded during catalytic conversion of hydroquinone using BRPD in presence of Zn^{2+} ions **d** Spectra recorded during degradation of catechol by BRPD

Table 2 BRPD activity of HQ in the presence of metals and inhibitors

	Activity (%)	concentration (μ M)
Metals		
Hg	96.5 ± 0.8	1 mM
Mg	70.17 ± 0.6	1 mM
Cu	35.08 ± 1.0	1 mM
Inhibitors		
4-HBA	98 ± 0.4	20 mM
Phenol	99 ± 0.7	20 mM
PNP	17.5 ± 0.5	20 mM

was found to be main discriminator for substrate binding in hydroquinone dioxygenases (Table 2).

Analysis of evolutionary conserved sequences

To understand molecular diversity and phylogenetic relatedness of BRPD, comprehensive sequence analysis was carried out and sequences showing > 30% similarity were used to

infer the evolutionary relationship. From phylogeny tree it becomes evident that it has large diversity at primary protein sequence level, and the homolog protein sequences representing Glyoxalase/ring-cleaving dioxygenase family can be divided into two major groups (Fig. 3a). Interestingly, we observed that metal ion centre (His9, His224 and Glu272, numbering according to our target sequence) is highly conserved (Fig. 3b). In addition, the metal ion coordinating residue His9 toward N- termini holds a highly conserved motif [G/X-X-H-H-X-T-A/X] while residue His224 toward C- terminal surrounds a highly conserved motif [G-X-X-H-H-X-A]. The secondary structure prediction using I-TASSER (Fig. S1) [28] predicted that BRPD contains four similar size $\beta\alpha\beta\beta$ modules, a highly conserved structural motif among the vicinal oxygen chelate (VOC) superfamily. This motif provides a metal co-ordinating environment connected by long loops in between. These repeating motifs span residues 7–63, 78–132, 158–207 and 223–275. The protein in this superfamily consists of $\beta\alpha\beta\beta$ modules, although the number and relative orientation of these modules can differ leading to structural diversity at 3D level [14]. BRPD amino acid sequences showed similarity

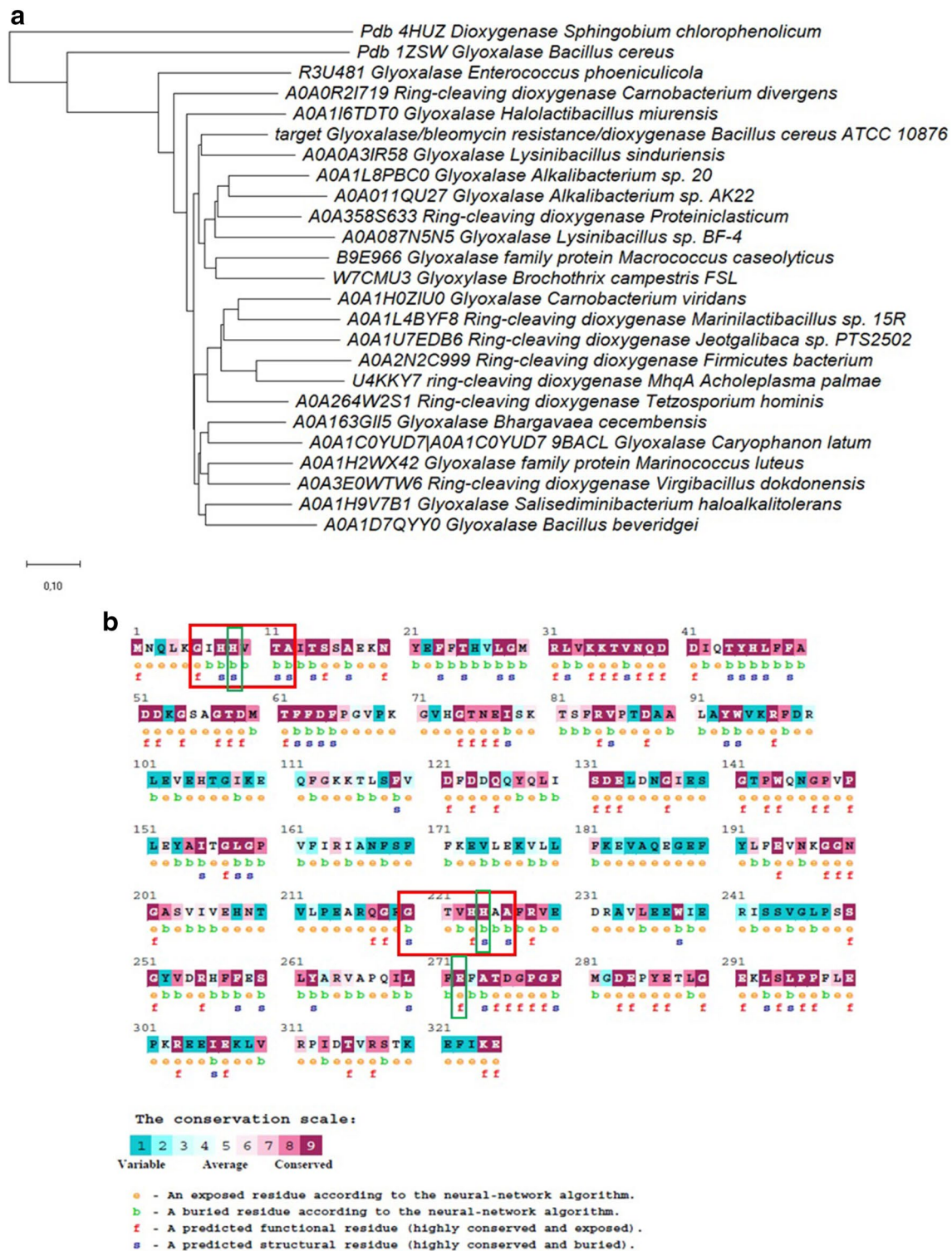


Fig. 3 a. Phylogenetic relatedness of targeted sequence (BRPD) and other related extradiol dioxygenases. All sequences were aligned using MUSCLE program with default settings. A distant neighbour joining tree was then created using the Mega (version 7.0). **b** Evolu-

tionary conserved sequences of BRPD, the red rectangle box shows the active site conserved motifs whereas the green rectangle box depicts the catalytic residues. (Color figure online)

with amino acids sequences of structural homologs for which 3D crystal structures are available (Fig. S2) and were used for building 3D model of BRPD as discussed below.

3D structural modelling, substrate docking and MD simulations

In order to investigate 3D structure of target protein, we performed structural molecular modelling and MD simulations with the modelled protein. Target sequence of BRPD showed ~39% and ~31% sequence identify with crystal structure of *Bacillus cereus* metallo protein (1ZSW) from glyoxalase family and crystal structure 2,6-dichloro-p-hydroquinone 1,2-dioxygenase (PcpA;4HUZ) protein from *Sphingobium chlorophenicum*, respectively. An average model obtained after 100 ns MD run and superimposed on template structure showed RMSD value corresponding to 1.15 Å. The overall structural topology retained the same conformation except some minor loop region flexibility in overall refine modelled structure after 100 ns MD run as depicted in Fig. 4a. The active site binding mode of tested substrates like Catechol and Hydroquinone were predicted

using the molecular docking studies. Both catechol and hydroquinone showed interactions with metal ion during substrate entry in the active site. The best docked conformation of catechol and hydroquinone into catalytic centre with metal ions distances is shown in Fig. 4b and c. We also performed structural modelling and MD simulations studies with two different metal ions Fe^{2+} and Zn^{2+} . During the entire 100 ns MD simulations the metal ions were found to be well coordinated with catalytic centre residues His9, His224 and His272. Furthermore the metal ion Fe^{2+} coordinates with three water molecules and catalytic residues His9, His224 and Glu272 and adopts the octahedral geometry while Zn^{2+} coordinates with two water molecules and catalytic residues His9, His224 and Glu272 and adopts the tetrahedral geometry. In both metal ions Fe^{2+} and Zn^{2+} consistency exhibited the bound average distance ~2.2 Å with NE2 atom of His9 and His224. Interesting, the side chain flexibly of Glu amino acid was observed and metal ion coordinates either OE1 or OE2 during the MD simulation in both metal ions as shown in Fig. 5a–d. Furthermore, we also predicted two putative binding sites for bleomycin in dioxygenase with similar

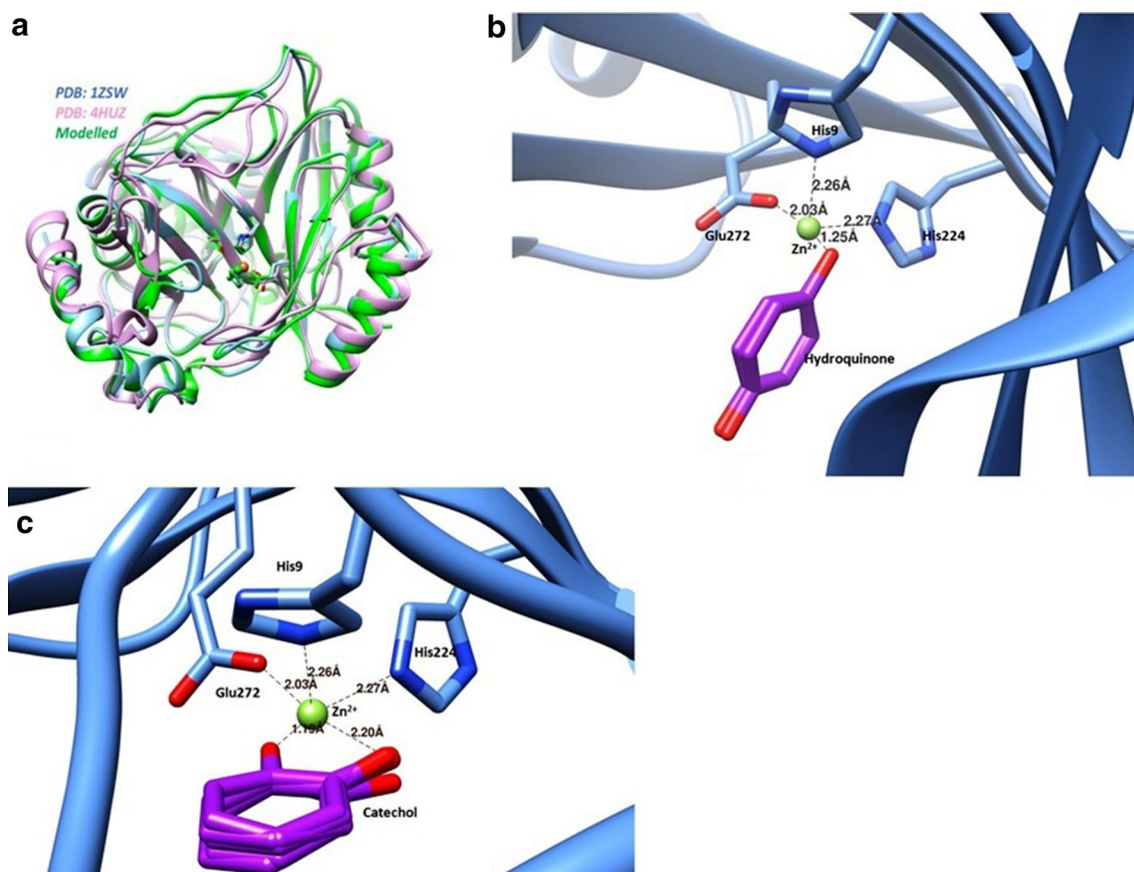


Fig. 4 In silico analysis of BRPD **a** An average modelled structure after 100 ns MD simulation showing bleomycin binding pocket. **b** Molecular docking of Hydroquinone. **c** Molecular docking of substrate catechol

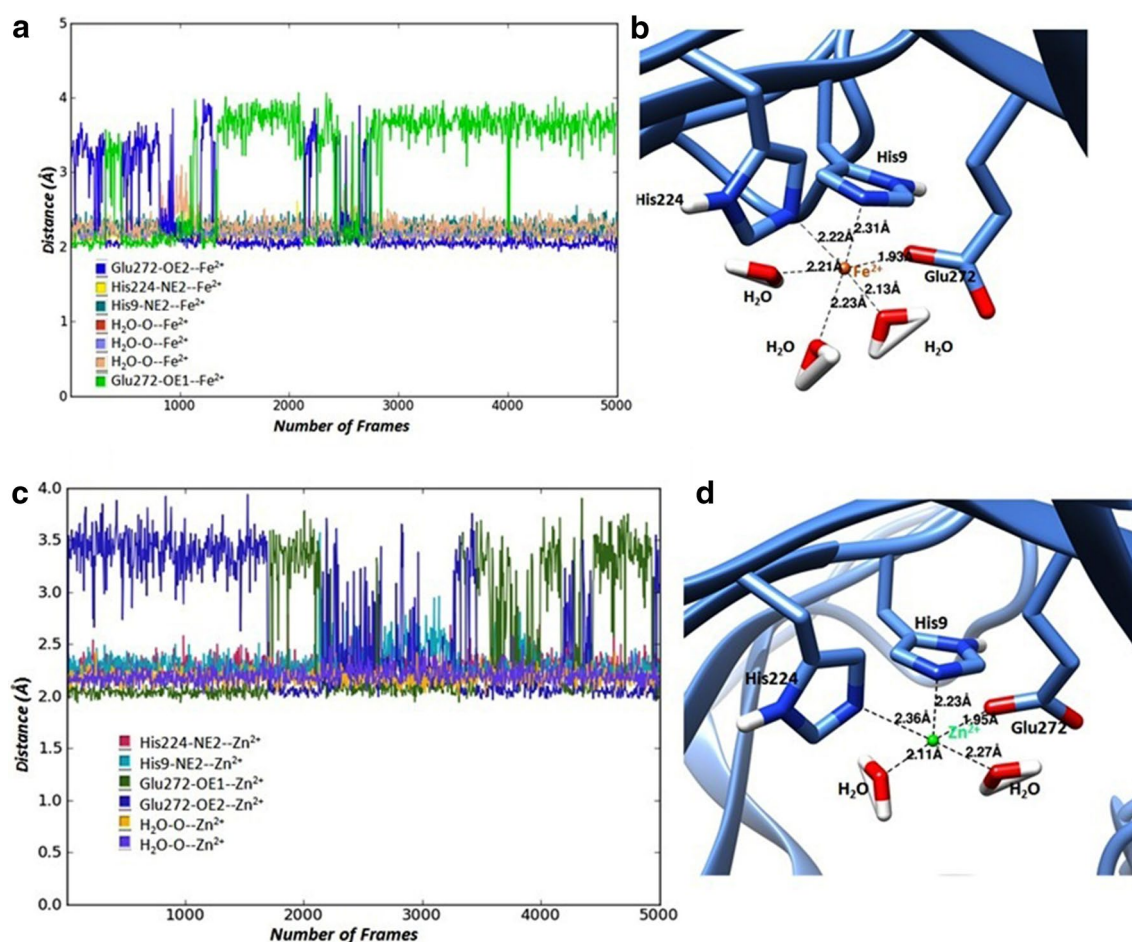


Fig. 5 **a**. The modeled protein simulated with Zn^{2+} metal ion representing distance between metal ion and co-ordinating residues, **b** The catalytic centre co-ordinated by Zn^{2+} , **c** the catalytic residues and water molecules during 100 ns MD simulation The modeled protein

simulated with Fe^{2+} metal ion showing distance between metal ion and coordinating residues, **d**: catalytic centre coordinated by Fe^{2+} , the catalytic residues and water molecules during 100 ns MD simulation

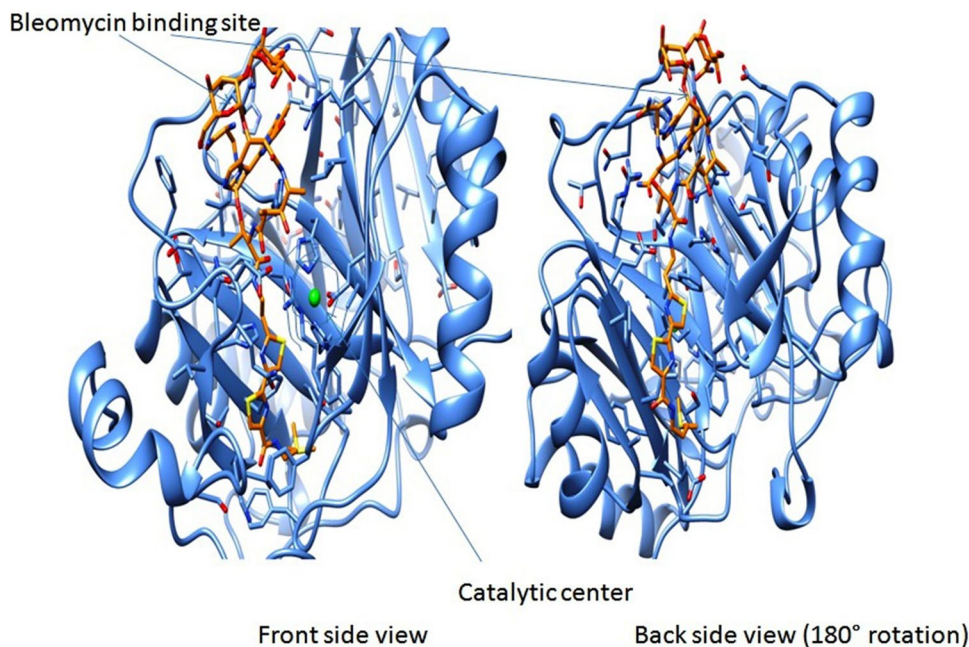
structural topology and cavity for binding of bleomycin as shown in Fig. 6.

Discussion

Hydroquinone dioxygenases (HQDO) are key enzymes that act on hydroquinone (HQ), a key intermediate of several aromatic hydrocarbons such as 4-nitrophenol [7], γ -hexachlorocyclohexane [8], 4-hydroxyacetophenone [9] and 4-aminophenol [10]. In the present investigation, we were able to isolate and characterize a novel hydroquinone dioxygenase from contaminated agricultural soil that catalyzes Fe^{2+} and Zn^{2+} dependent conversion of HQ (Hydroquinone) to 4-hydroxymuconic semialdehyde (320 nm). Interestingly, enzyme readily lost activity upon incubation with its substrate hydroquinone, which distinguishes it from PcpA and related hydroquinone dioxygenases [13] (Fig. S2). This may be attribute to oxidation of ferrous iron in the active

centre to ferric iron, a process which could be completely reversed within 32 h by reduction with 100 mM ascorbic acid (data not shown) and in vivo by redox-dependent reactions catalyzed by ferredoxins [38]. This characteristic feature is also reported previously for HQDO from *Sphingomonas* sp. strain TTNP3 [11], *Lactococcus lactis* IL1403 [39] and also for other extradiol type dioxygenases, such as catechol dioxygenases [40, 41] and protocatechuate dioxygenases [42]. However, like PcpA, BRPD also showed its dimeric nature (Fig. 1c) and further showed uneven faster movement on SDS-PAGE due to its acidic isoelectric point (pI 5.4; aspartic acid (D) and glutamic acid (E) content about ~16% of total protein) and also due to no cysteine amino acid residues in protein structure. Due to this, non-reduced protein nature causes BRPD like protein to unfold completely, retaining somewhat globular shape and bind to SDS less as compared to its mass and normally causes protein faster run on SDS-PAGE [43]. BRPD also shown very narrow optimal pH values ranging from 7.4 to 8.0 in phosphate buffer with no

Fig. 6 Predicated active site using the structural similarity and binding patterns of bleomycin. Frontal side view and back side view 180° rotation



activity was observed in the Tris buffer. Previously, MnpC, a hydroquinone dioxygenase involved in meta-nitrophenol degradation by *cupriavidus nectar* JMP134 showed amino acid homology and metals activity as well narrow pH range as similar to BRPD [23].

Molecular diversity and analysis of evolutionary conserved sequences revealed that both its N and C-terminal domains are conserved at sequence and structural level (Fig. S2). These domains shared strong similarity with the conserved domain of structurally related metalloproteins, including the bleomycin resistance protein, glyoxalase I, and type I ring-cleaving dioxygenases. It was observed that metal ion centre His9, His224 and Glu272 are highly conserved in this protein. In addition, the metal ion coordinating residue His9 toward N-termini hold a highly conserved motif [G/X-X-H-H-X-T-A/X] while residue His224 toward C-terminal surrounds a highly conserved motif [G-X-X-H-H-X-A]. As conserved amino acids in metal binding comes from topologically equivalent positions of the two modules i.e. from 1st and 4th module. Indeed, it was documented that formation of a symmetric protein with ability to bind a metal ion was a crucial step in the evolution of this family of proteins [44]. BRPD is activated in presence of divalent metal ions, with the most effective being Zn^{2+} and Fe^{2+} , and the overall order is $Zn^{2+} > Fe^{2+} > Hg^{2+} > Mg^{2+} > Cu^{2+}$. Previously, it was reported that this super family of proteins uses a variety of metal ions for their catalytic activities [16].

MD stimulations and docking studies using modelled BRPD provided constructive insights about arrangement of metal ion in the active site. It was observed that Fe^{2+} ion coordinates with three water molecules and catalytic residues

His9, His224 and Glu272, adopting octahedral geometry while Zn^{2+} ion adopts tetrahedral geometry by coordinating with two water molecules and catalytic residues. Both metal ions Fe^{2+} and Zn^{2+} consistently exhibited the bound average distance corresponding to $\sim 2.2 \text{ \AA}$ with NE2 atom of His9 and His224 (Fig. 4b, c). Interestingly, the side chain flexibility of Glu amino acid was observed and metal ion coordinates at either OE1 or OE2 during the MD simulation. This flexibility allows these metal ions to temporarily dissociate from the active-site, and is required for stereospecific reaction in glyoxalase 1 [45]. The arrangement of protein ligands around different metal ions is found to be unique in relation to their function in dioxygenase family proteins. For example, protein ligands arrangement around Zn^{2+} ion and Fe^{2+} is the same as for the Zn^{2+} ion of human GLO and for the Co^{2+} , Ni^{2+} , or Cd^{2+} ions bound to *E. coli* GLO except that tetrahedral arrangement instead of octahedral and vice versa. An octahedral or tetrahedral co-ordination geometry that leaves two or three positions to be filled by water molecules seems to be essential for proper functioning [46].

In human GLO, a transition state analogue binds with Zn^{2+} by occupying two *cis* positions and displacing the water [45]. In *E. coli* GLO, active metal ions (Co^{2+} , Ni^{2+} , and Cd^{2+}) have two water molecules occupying *cis* octahedral sites, however on binding with incorrect metal ion (Zn^{2+}) its geometry changed to trigonal bipyramidal that results in loss of enzyme activity [14]. Thus, it can be inferred that these structural geometries in dioxygenase are important to catalyze degradation of aromatic hydrocarbons [13, 47]. Interestingly, low level of dioxygenase activity observed in the presence of Cu^{2+} (Table 2) indicate combined copper/quinone stress in the bacterial community of our study sample,

as also observed in Gram positive bacterium *Lactococcus lactis* IL1403 [39]. Further, substrate docking studies with modelled BRPD (Fig. 4b, c) provided important insights about the similarities and differences between BRPD and the EDOs (extradiol dioxygenases). The model sufficiently highlighted the binding modes of both the catechol and hydroquinone in the active sites by co-ordinating through Zn^{2+} ions to attain reasonable geometry and other divalent metals as also reported previously ([13, 15]. Further, in case of Fe(II) ions, three water molecule and 2-His-1-carboxylate facial triad forms six-co-ordinate complex with hydroquinone and BRPD to form 4-hydroxymuconic semi aldehyde as reported previously [9, 15].

Our results further demonstrate that electron withdrawing and electron donating substituent's groups in the *para* position located adjacent to the cleaving site is main discriminator for substrate binding with BRPD and related HQDO [9, 11]. In our study, 4-nitrophenol containing electron donating functional (OH) groups in *para* position exhibited strong inhibitory effect on enzyme activity, whereas those having electron withdrawing group substituents in *para* position e.g., 4-HBA demonstrated weak or no inhibitory effects. Interestingly, those lacking substituents in *para* position such as phenol inhibited enzyme activity less than 2% (Table 2) as also reported previously [11]. These results suggest that the BRPD activity is affected both by electronic and steric constraints in the active site.

Inspection of the superimposed 3D structures of BRPD, 1ZSW, PcpA (4HUZ) revealed high sequence similarity around the active-site pocket (Fig.S2). Consequently, the first and fourth $\beta\alpha\beta\beta$ motifs generally showed higher sequence similarity than the second and third motifs (Fig. S1). Specifically, the Fe(II) and Zn(II) co-ordinating residues and critical residues in the second co-ordination sphere were completely conserved. As PcpA has capability to degrade hydroquinone and related analogous, while 1ZSW have no known functions. Interestingly BRPD demonstrate similar activity and substrate specificity like PcpA, thus constituting a unique class of hydroquinone dioxygenases. It also showed bleomycin resistance property which is unique function of this family of protein; however, "dual effect" of antibiotic resistance and aromatic degradation remained elusive in these types of proteins. For the first time, Santos et al. [3] reported this kind of activity from metagenomic clone CRB2 (1), which is extradiol dioxygenase, however mechanism of antibiotic resistance is not yet clear.

Information retrieved after multiple sequence alignment of BRPD (Fig. S2) and its superimposition study with available crystal structures, PcpA, 1ZSW (Fig. 4a) as well as from previously reported literature [5, 15, 44], we propose that domain must have swapped among the first and fourth $\beta\alpha\beta\beta$ modules between BRPD and PcpA like HQDOs type I as compared to first and third in type I EDOs (Extradiol Dioxygenases) and

bleomycin resistance protein (BRP) [48]. Due to this swapping, there could be criss-cross reversal between two modules of dioxygenases and BRP domain. As a result, it could be speculated that in BRPD, metal binding domain is used to bind and degrade aromatic compounds while other domain binds and sequester bleomycin. Due to this BRPD, PcpA, human glyoxalase I [49], Yeast glyoxalase I belong to a family of protein having four $\beta\alpha\beta\beta$ modules in one polypeptide [15]. It also shows how VOC superfamily protein allows very different as well as unique functions on a very similar protein scaffold. Further, at the level of the dimer, the similarity between BRPD and PcpA persists, and using superposition study BRPD dimer match the equivalent atoms in the PcpA dimer with minor loop variation (data not shown). Finally, we concluded that in these proteins, it is the dimer that provides the common stable structural unit. Interactions between the two $\beta\alpha\beta\beta$ modules that make up the active site "substructure" seems insufficient to give such close correspondence between BRPD and PcpA; rather it is the extensive interface between the backs of the two "substructure" (the BRPD dimer interface) that stabilizes the overall structure [13, 16]. Thus, a very stable BRPD-like dimer would provide the basis for domain swapping without disturbing structure and function.

Conclusion

For the first time, we propose a comprehensive picture of BRPD with its unique catalytic mechanism that is very unlikely conserved among the HQDO type I having capability to degrade hydroquinone, catechol as well resistance to antibiotic like bleomycin. Knowledge of the structure and biochemical characterisation reported here will be beneficial not only for the basic biochemistry of aromatic hydrocarbon metabolism, but also increases our knowledge on antibiotic resistance elements, especially those from natural environments.

Funding This research Grant was funded by the Science and Engineering Research Board (SERB) New Delhi, project file number: SB/YS/LS-63/2013 under fast track scheme for the young scientists. Dr PKS would like to thank SERB for financial support.

Compliance with ethical standards

Conflict of interest The authors declare that they have no conflict of interest.

References

- Zhang T, Wooster MJ, Green DC, Main B (2015) New field-based agricultural biomass burning trace gas, $PM_{2.5}$, and black carbon emission ratios and factors measured in situ at crop residue fires in Eastern China. *Atmos Environ* 121:22–34

2. Fu B, Xu T, Cui Z, Ng HL, Wang K, Li J, Li QX (2018) Mutation of phenylalanine-223 to leucine enhances transformation of benzo[a]pyrene by ring-hydroxylating dioxygenase of *Sphingobium* sp. FB3 by increasing accessibility of the catalytic site. *J Agric Food Chem* 66(5):1206–1213
3. Santos DF, Istvan P, Noronha EF, Quirino BF, Krüger RH (2015) New dioxygenase from metagenomic library from Brazilian soil: insights into antibiotic resistance and bioremediation. *Biotechnol Lett* 37(9):1809–1817
4. Arora PK, Kumar M, Chauhan A, Raghava GP, Jain RK (2009) OxDBase: a database of oxygenases involved in biodegradation. *BMC Res Notes* 2:67
5. Cole JR, Konstantinidis K, Farris RJ, Tiedje JM (2010) Microbial diversity and phylogeny: extending from rRNAs to genomes. In: Liu W-T, Jansson JK (eds) *Environmental molecular microbiology*. Caister Academic Press, Norfolk, pp 1–19
6. Spain JC, Gibson DT (1991) Pathway for biodegradation of para-nitrophenol in a *Moraxella* sp. *Appl Environ Microbiol* 57(3):812–819
7. Zhang S, Sun W, Xu L, Zheng X, Chu X, Tian J, Wu N, Fan Y (2012) Identification of the para-nitrophenol catabolic pathway, and characterization of three enzymes involved in the hydroquinone pathway, in *Pseudomonas* sp. 1-7. *BMC Microbiol* 12:27
8. Miyauchi K, Adachi Y, Nagata Y, Takagi M (1999) Cloning and sequencing of a novel meta-cleavage dioxygenase gene whose product is involved in degradation of gamma-hexachlorocyclohexane in *Sphingomonas paucimobilis*. *J Bacteriol* 181(21):6712–6719
9. Moonen MJH, Kamerbeek NM, Westphal AH, Boeren SA, Jansen DB, Fraaije MW, van Berkel WJH (2008) Elucidation of the 4 hydroxyacetophenone catabolic pathway in *Pseudomonas fluorescens* ACB. *J Bacteriol* 190(15):5190–5198
10. Takenaka S, Okugawa S, Kadowaki M, Murakami S, Aoki K (2003) The metabolic pathway of 4-aminophenol in *Burkholderia* sp strain AK-5 differs from that of aniline and aniline with C-4 substituents. *Appl Environ Microbiol* 69(9):5410–5413
11. Kolvenbach BA, Lenz M, Benndorf D, Rapp E, Fousek J, Vlcek C, Schäffer A, Gabriel FL, Kohler HP, Corvini PF (2011) Purification and characterization of hydroquinone dioxygenase from *Sphingomonas* sp. strain TTNP3. *AMB Express* 1(1):8
12. Eltis LD, Bolin JT (1996) Evolutionary relationships among extradiol dioxygenases. *J Bacteriol* 178(20):5930–5937
13. Hayes RP, Green AR, Nissen MS, Lewis KM, Xun L, Kang C (2013) Structural characterization of 2,6-dichloro-p-hydroquinone 1,2-dioxygenase (PcpA) from *Sphingobium chlorophenolicum*, a new type of aromatic ring-cleavage enzyme. *Mol Microbiol* 88(3):523–536
14. He P, Moran G (2011) Structural and mechanistic comparisons of the metal-binding members of the vicinal oxygen chelate (VOC) superfamily. *J Inorg Biochem* 105(10):1259–1272
15. Machonkin TE, Holland PL, Smith KN, Liberman JS, Dinescu A, Cundari TR, Rocks SS (2010) Determination of the active site of *Sphingobium chlorophenolicum* 2,6-dichlorohydroquinone dioxygenase (PcpA). *J Biol Inorg Chem* 15(3):291–300
16. McCarthy AA, Baker HM, Shewry SC, Patchett ML, Baker EN (2001) Crystal structure of methylmalonyl-coenzyme A epimerase from *P. shermanii*: a novel enzymatic function on an ancient metal binding scaffold. *Structure* 9(7):637–646
17. Dortet L, Girlich D, Virlouvet AL, Poirel L, Nordmann P, Iorga BI, Naas T (2017) Characterization of BRP_{MBL}, the bleomycin resistance protein associated with the carbapenemase NDM. *Antimicrob Agents Chemother* 61(3):2413–2416
18. Zhang JJ, Liu H, Xiao Y, Zhang XE, Zhou NY (2009) Identification and characterization of catabolic para-Nitrophenol 4-Monooxygenase and para-benzoquinone reductase from *Pseudomonas* sp. strain WBC-3. *J Bacteriol* 191(8):2703–2710
19. Shen W, Liu W, Zhang J, Tao J, Deng H, Cao H, Cui Z (2010) Cloning and characterization of a gene cluster involved in the catabolism of p-nitrophenol from *Pseudomonas putida* DLL-E4. *Bioresour Technol* 101(19):7516–7522
20. Min J, Zhang JJ, Zhou NY (2014) The gene cluster for para-Nitrophenol catabolism is responsible for 2-Chloro-4-Nitrophenol degradation in *Burkholderia* sp. strain SJ98. *Appl Environ Microbiol* 80(19):6212–6222
21. Dunwell JM, Purvis A, Khuri S (2004) Cupins: the most functionally diverse protein superfamily? *Phytochemistry* 65(1):7–17
22. Armstrong RN (2000) Mechanistic diversity in a metalloenzyme superfamily. *Biochemistry* 39(45):13625–13632
23. Yin Y, Zhou NY (2010) Characterization of MnpC, a hydroquinone dioxygenase likely involved in the meta-nitrophenol degradation by *Cupriavidus necator* JMP134. *Curr Microbiol* 61(5):471–476
24. Webb B, Sali A (2016) Comparative protein structure modeling using MODELLER. *Curr Protoc Bioinform* 86:2.9.1–2.9.37
25. Saitou N, Nei M (1987) The neighbor-joining method: a new method for reconstructing phylogenetic trees. *Mol Biol Evol* 4(4):406–425
26. Zuckerkandl E, Pauling L (1965) Evolutionary divergence and convergence in proteins. In: Bryson V, Vogel HJ (eds) *Evolving genes and proteins*. Academic Press, New York, pp 97–166
27. Kumar S, Stecher G, Tamura K (2016) MEGA7: molecular evolutionary genetics analysis version 7.0 for bigger datasets. *Mol Biol Evol* 33(7):1870–1874
28. Yang J, Yan R, Roy A, Xu D, Poisson J, Zhang Y (2015) The I-TASSER Suite: protein structure and function prediction. *Nat Methods* 12(1):7–8
29. Ashkenazy H, Abadi S, Martz E, Chay O, Mayrose I, Pupko T, Ben-Tal N (2016) ConSurf 2016: an improved methodology to estimate and visualize evolutionary conservation in macromolecules. *Nucleic Acids Res* 44(W1):W344–W350
30. Ashkenazy H, Erez E, Martz E, Pupko T, Ben-Tal N (2010) ConSurf 2010: calculating evolutionary conservation in sequence and structure of proteins and nucleic acids. *Nucleic Acids Res* 38(Web Server issue):W529–W533
31. Pettersen EF, Goddard TD, Huang CC, Couch GS, Greenblatt DM, Meng EC, Ferrin TE (2004) UCSF Chimera—a visualization system for exploratory research and analysis. *J Comput Chem* 25(13):1605–1612
32. Maier JA, Martinez C, Kasavajhala K, Wickstrom L, Hauser KE, Simmerling C (2015) ff14SB: improving the accuracy of protein side chain and backbone parameters from ff99SB. *J Chem Theory Comput* 11(8):3696–3713
33. Jorgensen WL, Chandrasekhar J, Madura JD (1983) Comparison of simple potential functions for simulating liquid water. *J Chem Phys* 79(2):926
34. Essmann U, Perera L, Berkowitz ML, Darden T, Lee H, Pedersen LG (1995) A smooth particle mesh Ewald method. *J Chem Phys* 103(19):8577–8593
35. Ryckaert JP, Ciccotti G, Berendsen HJC (1977) Numerical integration of the Cartesian equations of motion of a system with constraints: molecular dynamics of n-alkanes. *Comput Phys* 23(3):327
36. Kumar R, Shaikh N, Sharma S, Garg P (2015) A comparative study of integrase binding domain of homologous LEDGF/p75 and HRP2 protein: from sequence analysis to structural characterization. *Mol Simul* 41(8):683–690
37. Kumar R, Garg P (2013) Molecular modeling and active site binding mode characterization of aspartate β -semialdehyde dehydrogenase family. *Mol Inform* 32(4):377–383
38. Tropel D, Meyer C, Armengaud J, Jouanneau Y (2002) Ferredoxin-mediated reactivation of the chlorocatechol 2,3-dioxygenase from *Pseudomonas putida* GJ31. *Arch Microbiol* 177(4):345–351

39. Mancini S, Abicht HK, Gonskikh Y, Solioz M (2015) A copper-induced quinone degradation pathway provides protection against combined copper/quinone stress in *Lactococcus lactis* IL1403. *Mol Microbiol* 95(4):645–659
40. Cerdan P, Wasserfallen A, Rekik M, Timmis KN, Harayama S (1994) Substrate specificity of catechol 2,3-dioxygenase encoded by tol plasmid p_{WVO} of *Pseudomonas putida* and its relationship to cell-growth. *J Bacteriol* 176(19):6074–6081
41. Bartels I, Knackmuss HJ, Reineke W (1984) Suicide inactivation of catechol 2,3-dioxygenase from *Pseudomonas putida* mt-2 by 3-halocatechols. *Appl Environ Microbiol* 47(3):500–505
42. Ono K, Nozaki M, Hayaishi O (1970) Purification and some properties of protocatechuate 4,5-dioxygenase. *Biochim et Biophys Acta* 220(2):224–238
43. Guan Y, Zhu Q, Huang D, Zhao S, Jan Lo L, Peng J (2015) An equation to estimate the difference between theoretically predicted and SDS PAGE-displayed molecular weights for an acidic peptide. *Sci Rep* 5(1):13370
44. Bergdoll M, Eltis LD, Cameron AD, Dumas P, Bolin JT (1998) All in the family: structural and evolutionary relationships among three modular proteins with diverse functions and variable assembly. *Protein Sci* 7(8):1661–1670
45. Jafari S, Kazemi N, Ryde U, Irani M (2018) Higher flexibility of Glu-172 explains the unusual stereospecificity of glyoxalase I. *Inorg Chem* 57(9):4944–4958
46. Cameron AD, Olin B, Ridderstrom M, Mannervik B, Jones TA (1997) Crystal structure of human glyoxalase I -evidence for gene duplication and 3D domain swapping. *EMBO J* 16(12):3386–3395
47. Fetzner S (2012) Ring-cleaving dioxygenases with a cupin fold. *Appl Environ Microbiol* 78(8):2505–2514
48. Schlunegger MP, Bennett MJ, Eisenberg D (1997) Oligomer formation by 3D domain swapping: a model for protein assembly and misassembly. *Adv Protein Chem* 50:61–122
49. Saint-Jean AP, Phillips KR, Creighton DJ, Stone MJ (1998) Active monomeric and dimeric forms of *Pseudomonas putida* glyoxalase I: evidence for 3D domain swapping. *Biochemistry* 37(29):10345–10353

Publisher's Note Springer Nature remains neutral with regard to jurisdictional claims in published maps and institutional affiliations.